PROCEEDINGS OF SPIE

SPIEDigitalLibrary.org/conference-proceedings-of-spie

G-band FMCW Doppler radar for sea clutter and target characterization

Aleksanteri Vattulainen, Samiur Rahman, Duncan Robertson

Aleksanteri B. Vattulainen, Samiur Rahman, Duncan A. Robertson, "G-band FMCW Doppler radar for sea clutter and target characterization," Proc. SPIE 12108, Radar Sensor Technology XXVI, 121080T (27 May 2022); doi: 10.1117/12.2618497

SPIE.

Event: SPIE Defense + Commercial Sensing, 2022, Orlando, Florida, United States

G-band FMCW Doppler radar for sea clutter and target characterisation

Aleksanteri B. Vattulainen[a], Samiur Rahman[a], and Duncan A. Robertson[a]

[a]University of St Andrews, SUPA School of Physics and Astronomy, St Andrews, Scotland, United Kingdom

ABSTRACT

Marine autonomy is a field receiving a high degree of interest for its many potential applications in terms of commerce, crew safety, and the military. A successful autonomous vessel depends on a sophisticated degree of situational awareness facilitated by sensors. We are investigating sub-THz radar sensors for this purpose, with the primary goal being the characterization of sea clutter and targets in terms of both amplitude and Doppler statistics at frequencies spanning 24 to 350 GHz, where presently there is a lack of data. Sub-THz frequencies are of particular interest due to improved range and Doppler resolutions, and reduced sensor size, factors expected to be critical in enabling anomaly detection in the dynamic marine environment. As part of this work, a new 207 GHz frequency modulated continuous wave (FMCW) radar is being developed for the collection of clutter and target phenomenology data. The architecture uses a direct digital synthesis (DDS) generated chirp which is upconverted onto a low phase noise microwave LO then frequency multiplied by 24 to the carrier frequency. Twin Gaussian optics lens antennas (GOLAs) are used for transmit and receive with beamwidths of 2°, with adjustable linear polarization. The radar head is gimbal mounted for raster scanning RCS maps or for use in staring mode Doppler measurements. A chirp bandwidth of 4 GHz enables range bins of a few centimeters and high speed chirps enable a maximum unambiguous velocity of ±5 m/s.

Keywords: G-band, FMCW radar, Doppler radar, radar sea clutter, target characterization

1. INTRODUCTION

1.1 Motivation

There is a growing commercial interest in autonomous marine vessels, which will improve efficiency and personnel safety by reducing the need for crew and cabin space. This is relevant to all marine sectors, such as shipping and transportation, the military, and supply. Marine autonomy will require novel sensors for situational awareness, and radar is a stand out choice due to day/night operation and the ability to operate in obscuring conditions common at sea. Many of the benefits expected of marine autonomy parallel those of self-driving cars, where W-band automotive radar at 77 GHz is already an established sensor modality.

In the marine case however, higher frequency radar systems are of particular interest due to the greater range, cross-range and Doppler resolutions achievable with a compact antenna, where the greater fidelity is likely to be crucial in the dynamic marine environment. G-band radar is expected to reap these benefits, thus we are investigating its use for the measurement of sea clutter and the characterization of marine targets. This work is part of a broader project exploring this application using six radars operating at frequencies spanning 24-350 GHz.

Thorough sea clutter characterization is essential for situational awareness as it provides both direct information about the environment e.g. wave height, as well as being the first step in anomaly detection, functioning as the baseline for comparison of subsequent live data. Sea clutter is described by amplitude and Doppler statistical distributions which are affected by sea state (broadly speaking encapsulating wave height and surface roughness), wave direction, polarization, grazing angle, and radar frequency.[1] This multi-parameter dependence is due to the complex structure of the sea surface and the contributions of multiple radar scattering mechanisms this causes.[2] In general, there are very few published empirical data of sea clutter above Ka-band, and none whatsoever above W-band, hence a detailed study will expand the information available to the field. The most comprehensive collection of backscatter sea clutter data is Nathanson's Tables.[3]

Radar Sensor Technology XXVI, edited by Kenneth I. Ranney, Ann M. Raynal, Proc. of SPIE
Vol. 12108, 121080T · © 2022 SPIE · 0277-786X · doi: 10.1117/12.2618497

1.2 Prior Art

G-band radar has remained relatively exotic in comparison with lower mm-wave frequencies owing to the scarcity and/or expense of components needed, such as power amplifiers, mixers, and frequency multipliers. In principle however, it is attractive due to the benefits mentioned above and as some specific meteorological applications become possible.[4] Given these advantages, some of the earliest reported G-band radars were pulsed radar systems engineered from 1988-91 employing vacuum tube technology (specifically, extended interaction oscillators) for a variety of applications: the measurement of backscatter from trees at 215 GHz,[5,6] also used for cloud profiling;[7] tree backscatter measurements at 225 GHz,[8,9] also used for polarimetric measurements of natural surfaces;[10] and a coherent radar used for target detection and measurement of Doppler spectra.[11]

With the development of G-band solid-state components, there has been renewed interest in recent years as the smaller form factor, lower energy consumption and lower cost makes applications more practical at research level than with vacuum tubes, where improved commercial viability is expected to follow given the successful demonstration of the value of these systems. Applications include: a 220 GHz radar built in 2016 for concealed object detection;[12] a wideband on-chip transceiver for 210-270 GHz operation[13] also proposed for concealed object detection; and a cloud profiling and humidity sensing system named VIPR using the differential absorption radar principle, from which a number of publications have resulted from ongoing research.[14,15] These latter systems based on solid state technology are all FMCW, this mode of operation preserving SNR whilst accommodating the lower peak powers generated by solid state components. A notable advanced G-band radar is the 235 GHz video synthetic aperture radar ViSAR, reported in 2018, which combined state-of-the-art solid-state components with a traveling wave tube (TWT), to investigate the advantages of shorter wavelengths and reduced aperture time in high resolution imaging.[16]

Of the systems referenced here and above, all are incoherent except for that designed by Forsythe et al. in 1991,[11] ViSAR,[16] and VIPR which although capable of coherent measurements has only a maximum unambiguous velocity of ± 0.44 m/s.[17] Recently a new ground-breaking cloud profiling radar named GRaCE was published, using pulsed operation at 199.5 GHz with solid state components and capable of measuring Doppler velocities up to ± 9.38 m/s.[18] Doppler capable radar systems at G-band remain scarce.

In this paper, firstly an overview of the system requirements is presented. This is followed by a description of the resulting radar architecture, the system integration, and antenna design. Section 3 covers the characterization results of radar subsystems, including antenna S11 measurements, the output power of the transmit chain, and the noise figure of the receive chain, followed by the conclusion in Sec. 4.

2. DESIGN

2.1 Design Goals

A summary of the desired radar design specifications is included in Table 1. The center frequency of 207 GHz was chosen to be as close as possible to the atmospheric attenuation window at 220 GHz whilst constrained by the expected drop in transmit power of the available mm-wave components approaching 210 GHz. Bandwidth was similarly constrained at the upper extreme by component performance, where a value of 4 GHz (i.e. 3.75 cm range resolution) was chosen as a compromise.

The link budget was configured to give a clutter to noise ration (CNR) of -10 dB at a range of 100 m for the estimated transmit power of 14 dBm and noise figure of 9 dB. Clutter RCS scales with the size of the illuminated clutter patch, which is a function of clutter NRCS, beamwidth, grazing angle, and range. This was calculated using the method in Nathanson[3] for determining the area of a range-gated beam footprint, for a range of 100 m, grazing angle of 1°, a beamwidth of 2°, and an NRCS of -30 dB. This value was estimated from data in Nathanson's tables and following research conducted at 94 GHz.[19] The CNR is also a function of antenna gain, where this was optimized with regards to transmit power and the desired beamwidth. Further antenna design specifics are detailed in Subsection 2.3. System polarization is linear as dictated by available component waveguide interfaces. Polarization was desired to be adjustable to give HH, VV, HV, and VH as this has been shown to be a significant variable for sea clutter measurements. A maximum unambiguous Doppler of ± 5 m/s was determined to be sufficient for wave spectra, setting the required chirp repetition frequency (CRF). Whilst the DDS is capable of a greater CRF, this was avoided to reduce the impact to the instrument noisefloor.

Table 1: Estimated radar design parameters.

Center Frequency	207 GHz
Bandwidth/Range Resolution	4 GHz/3.75 cm
Transmit Power	14 dBm
Receiver Noise Figure	9 dB
Antenna Gain	39 dB
Antenna -3 dB Beamwidth	2° symmetric
Polarization	HH, VV, VH, HV
CRF	13.8 kHz
Maximum Unambiguous Doppler	±5 m/s

2.2 System Design

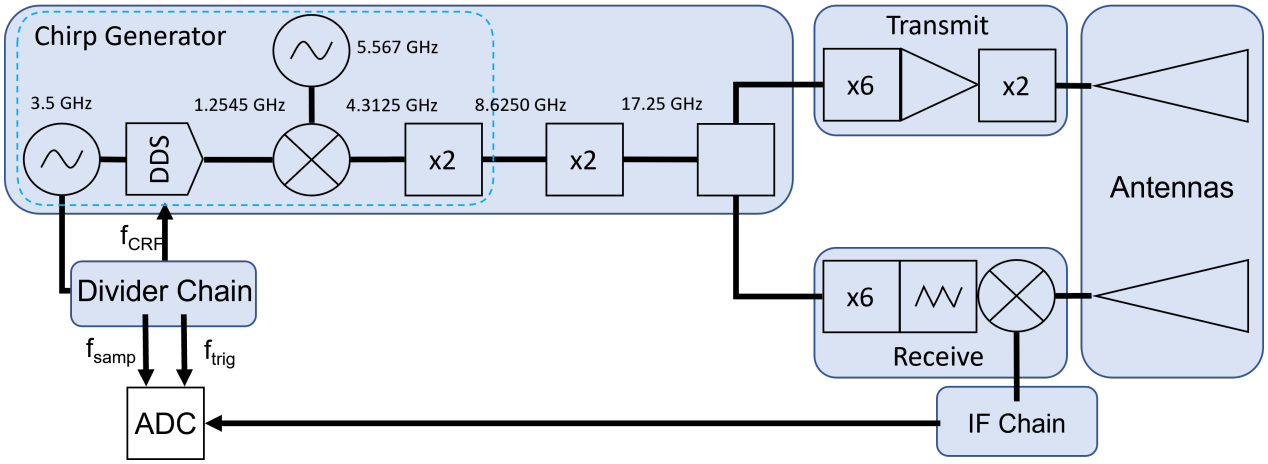

Figure 1: Simplified radar block diagram. ADC sampling and chirp generation via the DDS are clocked by the same 3.5 GHz DRO source. Chirps are upconverted by lower sideband mixing before further multiplication, amplification and filtering stages. The signal is then split between transmit and receive arms, undergoing further amplification and x12 frequency multiplication for transmit, and x6 frequency multiplication on receive. The receive signal provides the LO drive for a subharmonic mixer, which downconverts received RF to IF. This then undergoes amplification and filtering stages before sampling by the ADC.

A simplified radar design block diagram is shown in Fig. 1. The radar operates by upconverting a linearly frequency modulated (LFM) chirp produced by a DDS in the chirp generator stage, from a frequency center at 1.2545 GHz up to 4.3125 GHz with a dielectric resonator oscillator (DRO) signal at 5.567 GHz via a mixer selecting the lower sideband. This is then filtered, amplified and multiplied by 4 to a center frequency of 17.25 GHz. This previous design is the same as in Ref.[12] with the addition of a final doubling stage. Being DDS based this design has inherently low phase noise and high linearity, improving both the scatterer point response in down-range and the achievable Doppler resolution. Whilst the previous design was non-coherent, the coherent operation in the design presented here is achieved by using a second DRO at 3.5 GHz to clock the DDS chirp repetition frequency f_{CRF}, ADC trigger f_{trig} and to generate the ADC sampling signal f_{samp} via a division chain.

In the mm-wave stage, further multiplication with a Quantum Microwave frequency multiplier by a factor of 6 on each arm converts both transmit and receive signals to 103.5 GHz. On transmit a W-band Spacek Labs power amplifier (PA) drives a state-of-the-art commercial varactor diode doubler produced by Virginia Diodes

Inc. (VDI), generating the final 207 GHz signal for a total multiplication factor of 48. The receive arm features a Farran subharmonic mixer (SHM) using the 103.5 GHz signal as LO source for homodyne detection, where this downconverts RF from the antenna to an IF fed through two amplification stages and a low-pass filter prior to A/D conversion. The use of an SHM avoids the use of a second doubler for an LO signal, where the model used had an expected average conversion loss of 7-8 dB across the band, where this is still very good relative to a fundamental mixer.

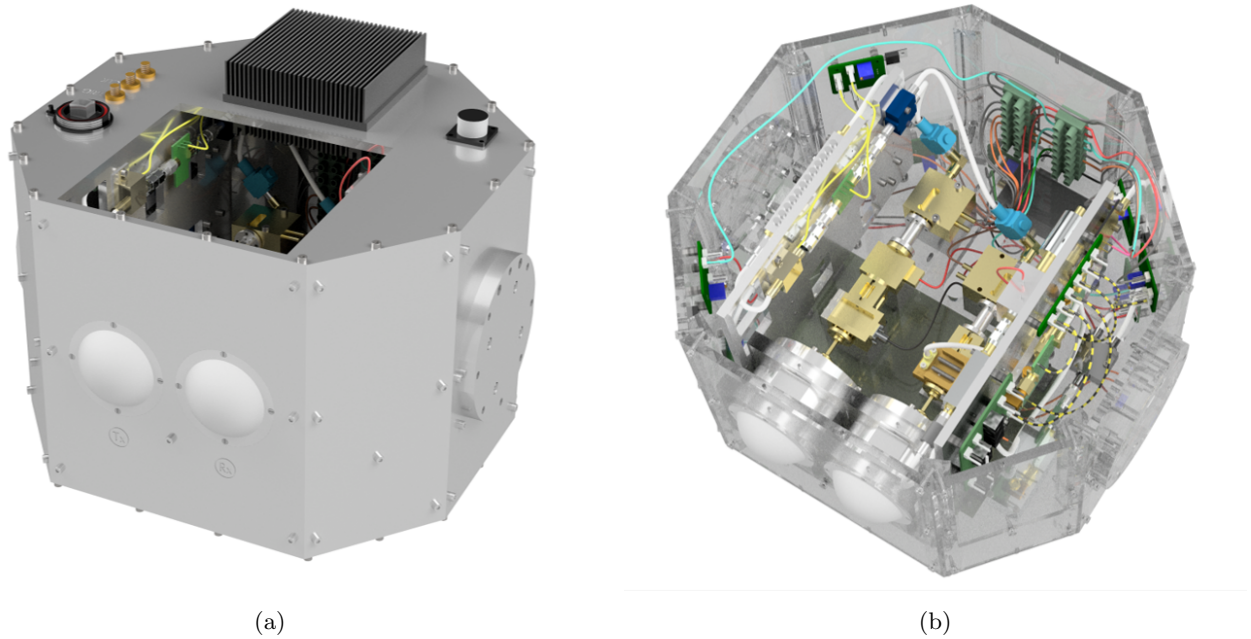

(a) (b)

Figure 2: Autodesk Inventor model of radar enclosure constructed from aluminum. The octagonal shape maximizes the available volume from within a sphere defined by the positioning gimbal whilst also being feasible to manufacture. The twin antennas mount through holes in the front face, with an opening on the top surface for an access hatch through which the antennas can be rotated to facilitate measurements in different polarizations.

As this radar is intended to be field deployable, the systems are designed to be well integrated and housed in a fairly weatherproof enclosure. A CAD model of this design is shown in Fig. 2. The radar is intended to be positioned in azimuth and elevation by a 2-axis gimbal, where the need to fit between two mounting flanges imposed some dimensional constraints resulting in the octagonal housing. An access hatch in the top plate of the housing allows for rotation of the antennas to allow measurement of different linear polarizations.

2.3 Antenna Design

Gaussian optics lens antennas (GOLAs) were chosen as these have a small form factor and could be manufactured in house at the University of St Andrews Workshop. Standalone horn antennas were considered however it was determined that horns of a sufficient gain would be too long to fit into the enclosure. The required gain was driven by the link budget detailed above and the trade-off between SNR and clutter patch area. A symmetric beamwidth of 2° was chosen to satisfy these criteria as well as allowing for ease of pointing. Separate GOLAs on the transmit and receive arms will provide adequate transmit/receive isolation.

The design of the GOLA horn is based on a linearized approximation of the spline profiles published by Granet.[20] These horns are composed of three conical sections with different flare angles, plus a rectangular-to-circular transition, which have been scaled down in size from those of a design proven at W-band to be appropriate for the required center frequency. This was first simulated using MATLAB running the mode-matching software CORRUG, which was then verified using a separate CST simulation. This simulation yielded a 3 dB beamwidth of 19° and a gain of 19.3 dBi for a standalone horn. Lenses were designed according to

equations from Goldsmith,[21] and the horn/lens system then simulated in CST for an edge taper of -32 dB. The planar-spherical lens design was selected over a planar-aspherical design given the results of the former were more favorable. The simulation predicted the required symmetric beamwidth of 2°, with a directivity of 39 dBi and a gain after accounting for material losses of 38.9 dB.

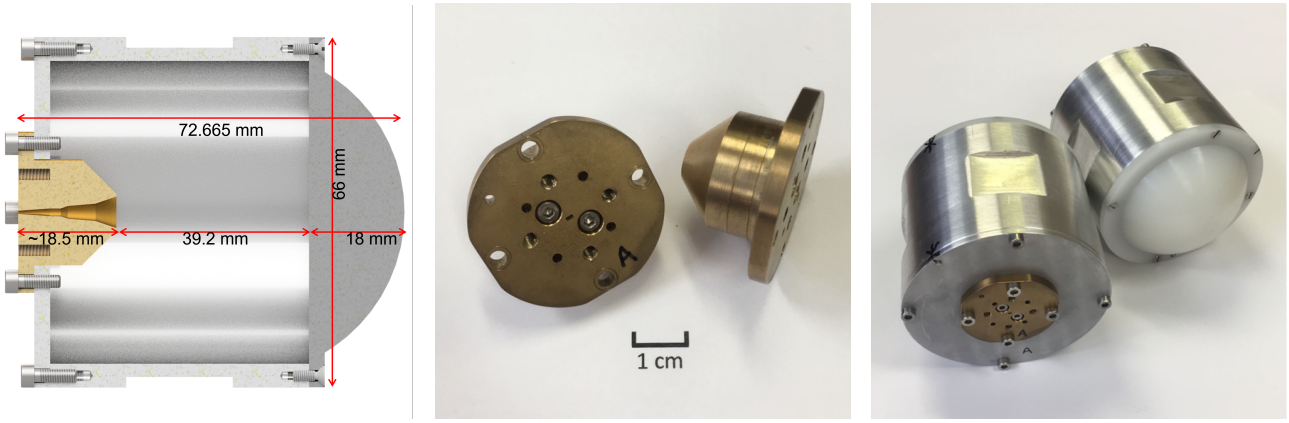

(a) (b) (c)

Figure 3: GOLA design and manufactured components. (a) Shows a cross-sectional view of the GOLA assembly, consisting of brass feedhorn, aluminum housing, and HDPE lens. (b) Shows both manufactured feedhorns and (c) shows both of the final assembled GOLAs.

The full GOLA design was subsequently modeled in Autodesk Inventor as seen in Fig. 3a. Figure 3b shows the horns which were manufactured from brass and fitted to an absorber lined aluminum assembly to provide the correct spacing between the horn and lens, which was machined from HDPE with a smooth finish (i.e. no additional impedance matching); both of the assembled GOLAs are shown shown in Fig. 3c.

3. CHARACTERIZATION RESULTS

3.1 Chirp Generator

The chirp generator used in this design follows the same design as used in Ref.[12] with the addition of a second doubling stage as the final element. The new design consists of a mixer upconversion stage, after which the signal is bandpass filtered, amplified and frequency doubled in two stages. This takes the DDS center frequency value from 1.2545 GHz to 4.3125 GHz after upconversion, and then to 17.25 GHz at the end of the chirp generator. To produce a final bandwidth of 4 GHz, the chirp bandwidth required from the DDS is 83.33 MHz, which at the end of the chirp generator increases to 333.33 MHz. The final bandwidth of 4 GHz is only 2% of the center frequency, whereas the original chirp generator was capable of up to 14% fractional bandwidth from between 200-230 GHz, which can be set by the DDS. The use of this design will allow for flexibility in center frequency and bandwidth for future research applications.

3.2 Divider Chain

The divider chain architecture is shown in Fig. 4. The chain is composed of three Analog Devices divider boards to derive f_{samp}; the HMC432 (divide by 2) performs the initial division to frequencies which can then be handled by the following HMC394 (divide by 11), where the second HMC394 (divide by 2) performs the rest of the required division whilst also restoring a 50/50 mark space ratio required by the ADC. The next division stage derives f_{CRF} for the DDS and f_{trig} for the ADC. This is accomplished by an Analog Devices DC1075B-A (divide by 4) to reduce the frequency to ≤ 20 MHz such that it is below the maximum clock frequency of the final division stage, a programmable divider board based on an Atmel ATmega168-PU microcontroller. The divided signal frequency and amplitude results were as expected, generating the required signals by the ADC and DDS chirps.

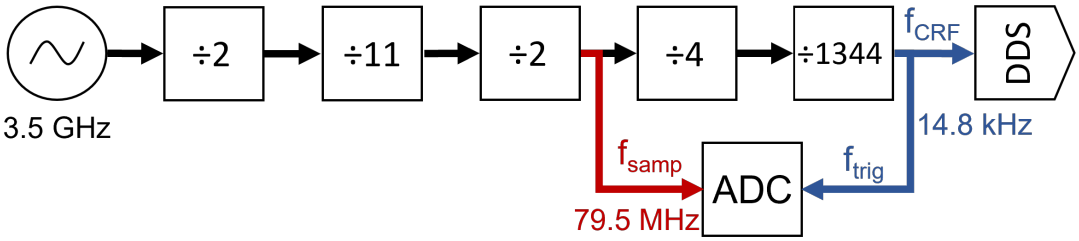

Figure 4: Divider chain block diagram.

3.3 Antenna S11 Measurements

The measured S11 of a horn and a fully assembled GOLA are plotted in Fig. 5, with the simulation results for the horn only since the CST simulation of the horn-lens combination had a prohibitively long run time. Simulation of the horn only was expected to be broadly applicable for this basic performance check as it is likely that the rectangular to circular transition would dictate the overall trend which would then be modulated by the presence of the lens.

The results show that the measured GOLA S11 approximately follows the trend of the horn S11, adding a standing wave modulation as it acts as a Fabry-Perot etalon. This adds a maximum positive variation of 2.3 dB versus the measured horn S11 in the region of interest, where compared to the simulation the greatest positive deviation is 4.3 dB. In general the measured horn S11 deviates from the simulation (in the position of the nulls most noticeably), however showing good agreement in the region of interest with a maximum deviation of 2.2 dB. Over the expected range of use the full GOLA S11 does not exceed -20 dB, giving no cause for concern regarding the final expected gain and beam pattern. These discrepancies are likely due to the expected manufacturing imperfections when producing such small components without dedicated micro-machining tools, where the greatest sources of error are expected to be any faults in the rectangular to circular transition or in the alignment of the horn sections. The addition of absorber lining inside the GOLA had minimal effect on the resulting S11 due to the very low edge taper of the horn-lens system, implying the cause of the standing wave modulation is reflection from the lens itself rather than the interior of the housing around it.

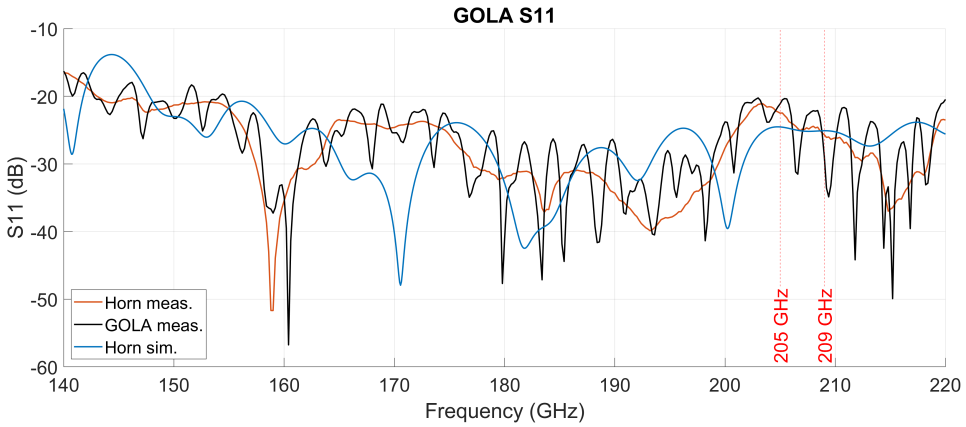

Figure 5: Measured S11 of the manufactured G-band feedhorn and full GOLA assembly compared with the CST simulation for the horn only.

3.4 Transmit Chain

The output power achieved from the Spacek Labs PA as a function of frequency is shown in Fig. 6a, with the proposed chirp bandwidth indicated. This provides the input signal at the correct level to drive the VDI doubler

which has been optimized for operation with a drive level of 19-21 dBm. The resulting G-band output power from the doubler is shown in Fig. 6b as measured with an absolute terahertz power/energy meter from Thomas Keating Ltd. Power peaks at 14.3 dBm at chirp center and varies by 0.5 dBm across the 4 GHz bandwidth. However the highest output is seen at 201.5 GHz with a value of 15.2 dBm, and this may justify lowering the center frequency. The measurement of G-band output power does not account for the loss in the feedhorn used to make the measurement, however once this is exchanged for the GOLA and associated waveguide link no more than an additional 0.5-1 dB loss is expected.

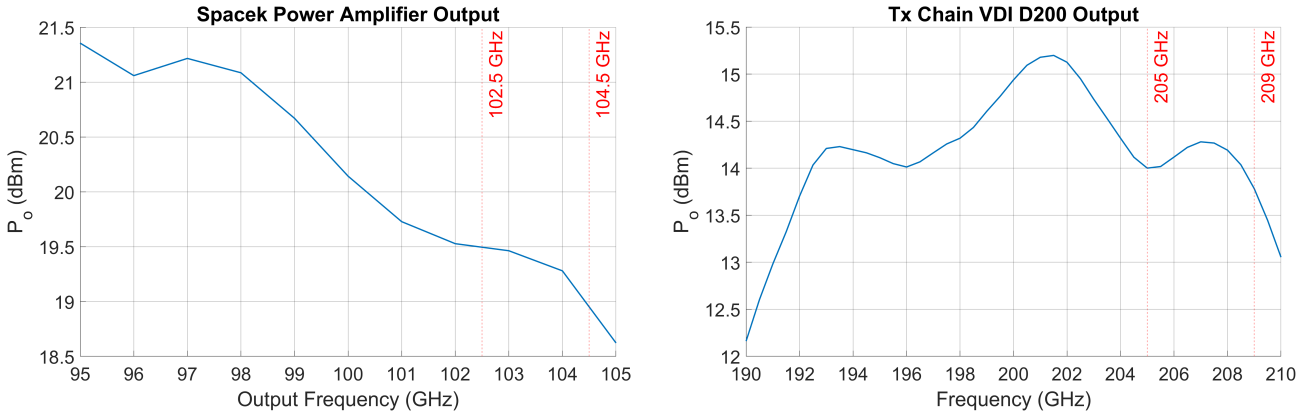

(a) (b)

Figure 6: (a) Shows the output power from the Spacek Labs power amplifier as part of the transmit chain as a function of frequency, (b) shows the output power of the VDI doubler driven by the output of the power amplifier.

3.5 Receive Chain

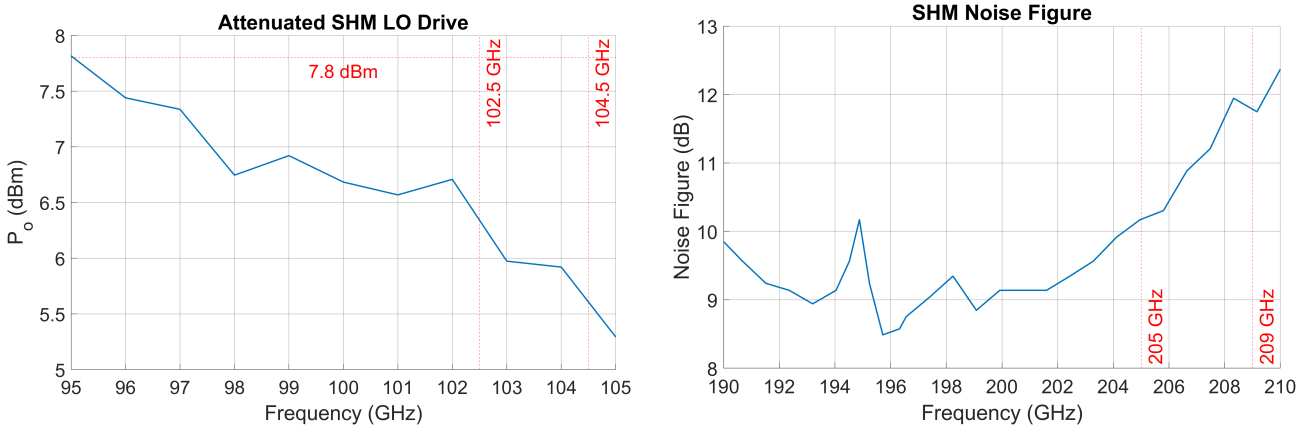

(a) (b)

Figure 7: (a) Shows the LO drive to the SHM as a function of frequency. This was limited to below the SHM operational limit of 7.8 dBm by the use of a 4 dB attenuator. (b) Shows the SHM noise figure as a function of RF frequency.

For the receive chain, testing determined the LO drive to be limited to below the 7.8 dBm maximum allowed by the mixer by using a 4 dB attenuator after the x6 multiplier, with the resulting curve shown in Fig. 7a. The noise figure was measured using the Y-factor method over a range of LO frequencies with a smooth conical horn on the RF port, and the results are shown in Fig. 7b. Again, this measurement does not account for the losses of the waveguide link and antenna on receive which will increase the noise figure by a further 0.5-1 dB. The noise figure shows significant variation across the measurement range, and across the proposed bandwidth: 11 dB at center frequency with a range of 1.8 dB. The chain of components attached to the IF port for the measurement have an extremely flat frequency response, thus the variation in the noise figure seen is due to the variation in

conversion loss of the SHM. The noise figure could be improved towards 9 dB by moving down to operate nearer 200 GHz. This, combined with the accompanying increase in transmit power, may offer a benefit to the radar signal budget of 2-3 dB over the current center frequency.

4. CONCLUSION

The design and build progress of a new G-band Doppler instrumentation radar has been presented. The primary goal of the radar is the characterization of sea clutter and marine targets to inform the design of future sub-THz radar sensors which will provide situational awareness for autonomous vessels. The radar employs a dual-antenna, homodyne FMCW architecture based around DDS chirp generation and frequency multiplication using advanced solid-state components.

Over the design frequency range of 205-209 GHz, the measured available transmit power from the varactor doubler is approximately 14 dBm, as designed. The receiver, which uses a subharmonic mixer front end, will have a noise figure of approximately 11-13 dB across the band, once antenna losses are included. This level of performance, whilst slightly worse than the design goal of ∼9 dB as stated in Tab. 1, should still enable our goal of data collection from the marine environment in the ∼100 m range.

The chirp generator is capable of a much wider bandwidth, however, and potentially allows operation over 190 to 210 GHz, providing flexibility in the actual choice of center frequency. Operating closer to 200 GHz may afford both an increase in transmit power of ∼1 dB and a reduction in noise figure of ∼2 dB so could improve radar sensitivity by ∼3 dB. This optimization will be conducted once system testing takes place. Note that operating at frequencies much below 200 GHz risks being affected by the increase in atmospheric absorption due to the 183 GHz molecular resonance. The radar bandwidth can also be reconfigured for different research applications such as other target and clutter phenomenology studies and atmospheric propagation research.

Ongoing development of the radar, to be reported in future publications, will include measurement of the antenna radiation patterns, characterization of the phase noise performance of the chirp generator, system integration and testing, and radar calibration. This will be followed by a campaign of field deployment, along with several other radars in the range 24 to 350 GHz to collect target and sea clutter data for analysis and algorithm development to support future marine autonomy.

ACKNOWLEDGMENTS

The authors acknowledge the financial support from the UK Engineering and Physical Science Research Council (EPSRC) under grant number EP/S032851/1.

REFERENCES

[1] Ward, K. D., Tough, R. J., and Watts, S., [*Sea clutter: Scattering, the K distribution and radar performance*] (2006).

[2] Raynal, A. M. and Doerry, A. W., "Doppler Characteristics of Sea Clutter," Tech. Rep. June, Sandia National Laboratories (2010).

[3] Nathanson, F. E., Reilly, J. P., and Cohen, M. N., [*Radar design principles: Signal Processing and the Environment*] (1991).

[4] Battaglia, A., Westbrook, C. D., Kneifel, S., Kollias, P., Humpage, N., Löhnert, U., Tyynelä, J., and Petty, G. W., "G band atmospheric radars: New frontiers in cloud physics," *Atmospheric Measurement Techniques* **7**, 1527–1546 (6 2014).

[5] McIntosh, R. E., Narayanan, R. M., Mead, J. B., and Schaubert, D. H., "Design and Performance of a 215 GHz Pulsed Radar System," *IEEE Transactions on Microwave Theory and Techniques* **36**(6), 994–1001 (1988).

[6] Narayanan, R. M., Borel, C. C., and McIntosh, R. E., "Radar Backscatter Characteristics of Trees at 215 GHz," *IEEE Transactions on Geoscience and Remote Sensing* **26**(3), 217–228 (1988).

[7] Mead, J. B., Mcintosh, R. E., Vandemark, D., and Swift, C. T., "Remote Sensing of Clouds and Fog with a 1.4-mm Radar," *Journal of Atmospheric and Oceanic Technology* **6**, 1090–1097 (12 1989).

[8] Mead, J. B. and McIntosh, R. E., "A 225 GHz polarimetric radar," *IEEE Transactions on Microwave Theory and Techniques* **38**, 1252–1258 (9 1990).

[9] Mead, J. B. and McLntosh, R. E., "Polarimetric Backscatter Measurements of Deciduous And Coniferous Trees at 225 GHz," *IEEE Transactions on Geoscience and Remote Sensing* **29**(1), 21–28 (1991).

[10] Mead, J. B., Langlois, P. M., Chang, P. S., and McIntosh, R. E., "Polarimetric Scattering from Natural Surfaces at 225 GHz," *IEEE Transactions on Antennas and Propagation* **39**(9), 1405–1411 (1991).

[11] Forsythe, R. E., Bohlander, R. A., and Butterworth, J. C., "An Experimental 225 GHz Pulsed Coherent Radar," *IEEE Transactions on Microwave Theory and Techniques* **39**(3), 555–562 (1991).

[12] Robertson, D. A., Macfarlane, D. G., and Bryllert, T., "220GHz wideband 3D imaging radar for concealed object detection technology development and phenomenology studies," *Passive and Active Millimeter-Wave Imaging XIX* **9830**(May 2016), 983009 (2016).

[13] Grzyb, J., Statnikov, K., Sarmah, N., Heinemann, B., and Pfeiffer, U. R., "A 210-270-GHz Circularly Polarized FMCW Radar with a Single-Lens-Coupled SiGe HBT Chip," *IEEE Transactions on Terahertz Science and Technology* **6**, 771–783 (11 2016).

[14] Cooper, K. B., Roy, R. J., Dengler, R., Monje, R. R., Alonso-Delpino, M., Siles, J. V., Yurduseven, O., Parashare, C., Millan, L., and Lebsock, M., "G-Band Radar for Humidity and Cloud Remote Sensing," *IEEE Transactions on Geoscience and Remote Sensing* **59**, 1106–1117 (2 2021).

[15] Roy, R. J., Lebsock, M., Millán, L., and Cooper, K. B., "Validation of a G-band differential absorption cloud radar for humidity remote sensing," *Journal of Atmospheric and Oceanic Technology* **37**(6), 1085–1102 (2020).

[16] Kim, S. H., Fan, R., and Dominski, F., "ViSAR: A 235 GHz radar for airborne applications," *2018 IEEE Radar Conference, RadarConf 2018* , 1549–1554 (6 2018).

[17] Cooper, K. B., Beauchamp, R. M., Roy, R. J., Millan, L., Lebsock, M. D., and Monje, R. R., "Cloud Dynamics Revealed by a G-band Humidity-Sounding Differential Absorption Radar," *IEEE National Radar Conference - Proceedings* **2020-September**, 0–4 (2020).

[18] Courtier, B. M., Battaglia, A., Huggard, P. G., Westbrook, C., Mroz, K., Dhillon, R. S., Walden, C. J., Howells, G., Wang, H., Ellison, B. N., Reeves, R., Robertson, D. A., and Wylde, R. J., "First Observations of G-Band Radar Doppler Spectra," *Geophysical Research Letters* **49**, e2021GL096475 (2 2022).

[19] Stove, A. G., Robertson, D. A., and Macfarlane, D. G., "Littoral sea clutter returns at 94GHz," in [*2014 International Radar Conference, Radar 2014*], Institute of Electrical and Electronics Engineers Inc. (3 2014).

[20] Granet, C., Bolton, R., and Moorey, G., "A smooth-walled spline-profile horn as an alternative to the corrugated horn for wide band millimeter-wave applications," *IEEE Transactions on Antennas and Propagation* **52**, 848–854 (3 2004).

[21] Goldsmith, P. F., [*Quasioptical systems: Gaussian beam quasioptical propagation and applications*] (1998).